Theoretical evaluation of a short-pulse electron-beam-excited XeF($B \rightarrow X$) laser using a low-pressure, room-temperature Ar/Xe/F_2 gas mixture

Naoto Nishida[a)]
Department of Electrical Engineering and Computer Science, Rice University, Houston, Texas 77251

Toshiaki Takashima
Department of Electrical Engineering, Faculty of Science and Technology, Keio University, 3-14-1 Hiyoshi, Kouhoku-ku Yokohama 223, Japan

Frank K. Tittel
Department of Electrical Engineering and Computer Science, Rice University, Houston, Texas 77251

Fumihiko Kannari and Minoru Obara[b)]
Department of Electrical Engineering, Faculty of Science and Technology, Keio University, 3-14-1 Hiyoshi, Kouhoku-ku Yokohama 223, Japan

(Received 21 July 1989; accepted for publication 20 December 1989)

A simulation code for an electron-beam-excited XeF($B \rightarrow X$) laser using Ar/Xe/F_2 gas mixtures is described. The validity of the code was checked by comparing the computed results to those obtained in a previously reported experiment with a 65-ns, 1.14-MW/cm^3 excitation pulse. Good agreement is demonstrated for sidelight fluorescence, laser waveforms, output power, and energy. Furthermore, the simulation code analysis suggests that the XeF laser can be operated effectively with low-pressure (<1 atm) Ar/Xe/F_2 mixtures at room temperature. A maximum intrinsic efficiency of $\sim 3\%$ is obtained at a total pressure of 0.5 atm. Such a low-pressure Ar/Xe/F_2 laser gas mixture would permit operation of a scaled-up XeF laser system since the intrinsic efficiency is as high as that with conventional high-pressure (~ 3 atm) Ne/Xe/NF_3 mixtures.

I. INTRODUCTION

The electron-beam- (e-beam-) pumped XeF($B \rightarrow X$) laser efficiency can be improved by means of (1) a gas mixture which has small photoabsorption coefficients and collisional quenching rates for XeF*,[1,2] (2) a high initial gas temperature,[3–5] and (3) high-energy density excitation.[6] Many experiments have been performed with Ne/Xe/NF_3 laser gas mixtures at around 3-atm total pressure because Ne-diluted gas mixtures have been considered to be more effective than Ar-diluted gas mixtures. Litzenberger and Mandl[5] obtained a maximum efficiency of 6% for a 3-amagat Ne/Xe/NF_3 laser gas mixture at an initial gas temperature of 425 K and with 500-ns, 300-kW/cm^3 excitation.

Scaling of a XeF ($B \rightarrow X$) excimer laser for fusion or remote sensing applications cannot be achieved by scaling of the gain length because of nonsaturable photoabsorption effects. Therefore, a large aperture is required for a scaled-up power amplifier, and such a laser should use low-pressure laser gas mixtures[7] which relax the design constraints for laser optics and e-beam diode foils. Furthermore, it is preferable to use a room-temperature gas mixture for a large-scale laser system because a high-temperature gas mixture causes optical distortions in large-aperture windows and/or the gas mixture itself.

In a previous paper[8] we reported on a comparative study of the XeF($B \rightarrow X$) laser efficiency using four different low-pressure gas mixtures at room temperature, i.e., 710-Torr Ar/Xe/F_2, 710-Torr Ar/Xe/NF_3, 1170-Torr Ne/Xe/F_2, and 1170-Torr Ne/Xe/NF_3. All mixtures were pumped at the same high excitation rate of 1.14 MW/cm^3 with a 65-ns e-beam current pulse. We found that the measured intrinsic efficiency of all four mixtures was $\sim 2\%$ in this low-pressure range.

At total pressures around 1 atm, an Ar-diluted gas mixture is more efficient in depositing the electron-beam energy into the laser gas mixture than a Ne-diluted mixture because of its higher stopping power. Figures 1(a) and 1(b) show calculated ion-ion recombination rate coefficients[9] as a function of total gas pressure. Figure 1(a) depicts the rate constants for the major XeF* formation process: $Xe^+ + F^- + M \rightarrow XeF^* + M$, and Fig. 1(b) important intermediate processes that form XeF* such as $Ne^+ + F^- + Ne \rightarrow NeF^* + Ne$ and $Ar^+ + F^- + Ar \rightarrow ArF^* + Ar$. Also, more Ar ions are produced than Ne ions for the same e-beam-power deposition since the energy loss per ion pair produced is 26 and 36 eV for Ar and Ne, respectively. The Ar diluent is considered to be more effective than the Ne diluent to form XeF* at total pressures below 2 atm. Only a small difference in laser performance was found for F_2 and NF_3, and F_2 is more suitable for high-repetition-rate operation.[10,11] Therefore, for a large-scale XeF laser system, an Ar/Xe/F_2 gas mixture will be most suitable.

A computer simulation is very useful to study the operational characteristics of the laser with wide variations of laser parameters. Theoretical analyses of the XeF($B \rightarrow X$) laser based on computer simulation were reported by Johnson, Palumbo, and Hunter,[12] Blauer *et al.*,[13] Moratz,

[a)] Present address: Manufacturing Engineering Lab., Toshiba Corp., 8, Shinsugita-cho, Isogo-ku, Yokohama 235, Japan.
[b)] To whom all correspondence should be addressed.

 0021-8979/90/093932-09$03.00 © 1990 American Institute of Physics

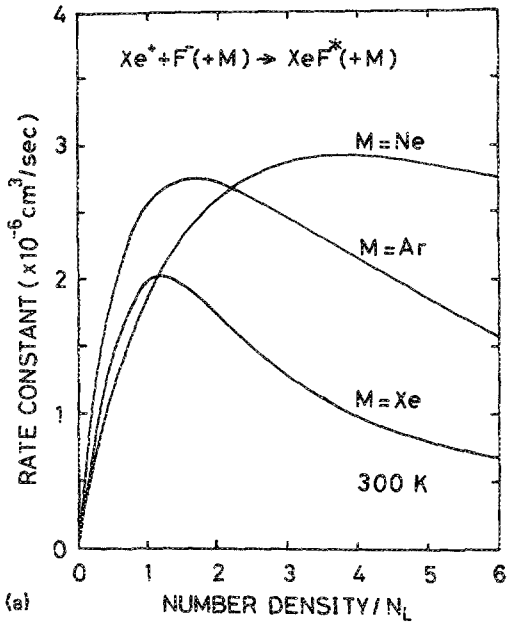

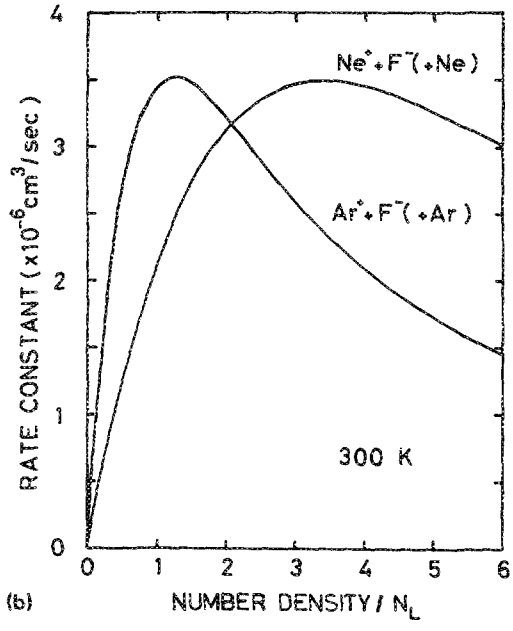

FIG. 1. Calculated ion-ion recombination rate constants at 300 K as a function of the number density of the third collision atoms (M): (a) $Xe^+ + F^- (+M) \rightarrow XeF^*(+M)$, M = Ne, Ar, and Xe; (b) $Ar^+ + F^-(+Ar) \rightarrow ArF^*(+Ar)$, and $Ne^+ + F^-(+Ne)$. Loschmidt number: $N_L = 2.67 \times 10^{19}\ cm^{-3}$.

Sawnders, and Kushner.[14] However, in these models Ne/Xe/NF_3 or Ne/Xe/F_2 laser gas mixtures with long pulse ($\sim 1\ \mu s$), low-density ($\sim 100\ kW/cm^3$) excitation were investigated.

This paper describes a comprehensive computer code for an *e*-beam-excited XeF($B \rightarrow X$) laser using an Ar/Xe/F_2 gas mixture for intense short-pulse excitation conditions. The model prediction using this code is in quite good agreement with former experimental results.[8] The intrinsic efficiency can be improved when the laser is operated below 1-atm total pressure where the formation rates of

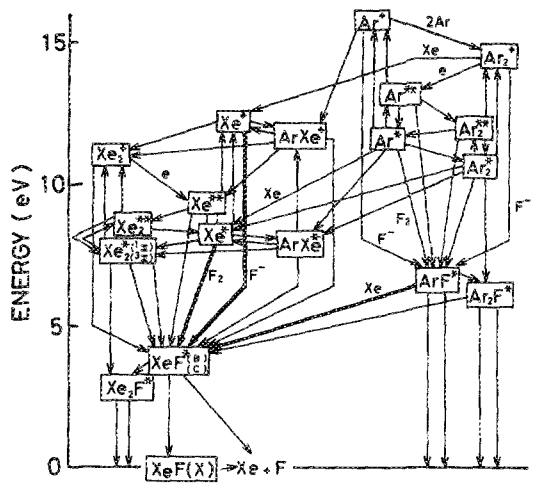

FIG. 2. Energy flow diagram for an Ar/Xe/F_2 laser gas mixture. The bold line shows the dominant pumping reaction channel for the XeF* (*B* and *C*).

photoabsorbers are small, and as a result, the laser extraction efficiency is greatly improved compared to that of 2-atm mixtures. A maximum intrinsic efficiency of 3% can be obtained at a total gas pressure of 0.5 atm and at room temperature according to the model prediction. This value is as high as that obtained with a conventional gas mixture, i.e., 3-atm Ne/Xe/NF_3, and therefore it is possible to use Ar/Xe/F_2 gas mixtures efficiently in a large-scale laser system.

In the following sections details of the model and the validity of the simulation code are described.

II. MODELING

The main kinetic channels in an Ar/Xe/F_2 mixture are summarized in Fig. 2. The dominant pumping reaction channels for XeF* are ion-ion recombinations, neutral reactions, and displacement reactions.

The numerical model in this paper is basically similar to the *e*-beam-excited XeCl laser model reported by Kannari *et al.*[15] The model consists of calculations for *e*-beam deposition, electron temperature, electron reaction rate, and chemical laser kinetics codes, which can predict the time-dependent laser performance as well as the optical gain and absorption characteristics.

Rate equations for each reaction and process are solved by a fourth-order Runge–Kutta method. All the reaction processes and the rate constants involved in this model are shown in Table I.[16–68] The ionization, excitation, and quenching reactions of the rare gases with secondary electrons are considered functions of the electron temperature. The temporal secondary-electron temperature is calculated assuming that the secondary-electron energy distribution is Maxwellian because of the extremely fast electron-electron collisions in a mixture of rare gas and halogen excited by an intense *e*-beam, in which the electron temperature is relatively low (1–2 eV) and the electron density is high (10^{14}–10^{15} #/cm^3).[15,69,70] The major XeF* formation channels are treated as functions of gas pressure and temperature.

The XeF($B \rightarrow X$) laser involves electronic transitions between an upper state *B* and a lower state *X*. Furthermore,

TABLE I. A list of reaction rate constants used in the computer simulation for the short-pulse e-beam-excited XeF($B \rightarrow X$) laser with Ar/Xe/F_2 gas mixture. T_e and T_g indicate electron temperature and gas temperature, respectively.

Reaction	Rate constant	Reference
Electron reaction		
$Xe + e_p \rightarrow Xe^+ + e_p + e_s$	21.7 eV/electron-ion pair	16
$Xe + e_p \rightarrow Xe^* + e_p$	49 eV/excited atom	17
$Ar + e_p \rightarrow Ar^+ + e_p + e_s$	26.4 eV/electron-ion pair	16
$Ar + e_p \rightarrow Ar^* + e_p$	93 eV/excited atom	17
$Xe + e_s \rightleftarrows Xe^* + e_s$	$3.41(-9)T_e 0.803\ \exp(-11.8/T_e)\text{cm}^3/\text{s}$	18
$Xe + e_s \rightleftarrows Xe^{**} + e_s$	$2.61(-8)T_e 0.0273\ \exp(-14.4/T_e)\text{cm}^3/\text{s}$	18
$Xe^* + e_s \rightleftarrows Xe^{**} + e_s$	$3.13(-7)T_e 0.803\ \exp(-2.06/T_e)\text{cm}^3/\text{s}$	18
$Xe + e_s \rightarrow Xe^+ + 2e_s$	$1.92(-8)T_e 0.80\ \exp(-18.0/T_e)\text{cm}^3/\text{s}$	18
$Xe^* + e_s \rightarrow Xe^+ + 2e_s$	$2.27(-7)T_e 0.117\ \exp(-6.21/T_e)\text{cm}^3/\text{s}$	18
$Xe^{**} + e_s \rightarrow Xe^+ + 2e_s$	$6.23(-7)T_e 0.12\ \exp(-3.60/T_e)\text{cm}^3/\text{s}$	18
$Xe_2^* + e_s \rightarrow Xe_2^+ + e_s$	$2.83(-7)T_e 0.12\ \exp(-5.10/T_e)\text{cm}^3/\text{s}$	18
$Xe_2^* + e_s \rightarrow 2Xe + e_s$	$1.0(-7)\text{cm}^3/\text{s}$	estimated
$Xe_2^* + e_s \rightarrow Xe_2^{**} + e_s$	$1.0(-7)\text{cm}^3/\text{s}$	17
$Xe_2^*(^3\Sigma) + e_s \rightarrow Xe_2^*(^1\Sigma) + e_s$	$8.8(-8)\text{cm}^3/\text{s}$	17
$Xe_2^*(^1\Sigma) + e_s \rightarrow Xe_2^*(^3\Sigma) + e_s$	$3.0(-7)\text{cm}^3/\text{s}$	17
$Xe_2^{**} + e_s \rightarrow Xe_2^*(^3\Sigma) + e_s$	$1.0(-6)\text{cm}^3/\text{s}$	17
$Xe_2^{**} + e_s \rightarrow Xe_2^*(^1\Sigma) + e_s$	$3.0(-7)\text{cm}^3/\text{s}$	17
$Ar + e_s \rightleftarrows Ar^* + e_s$	$3.70(-9)T_e^{0.74}\exp(-17.4/T_e)\text{cm}^3/\text{s}$	19
$Ar + e_s \rightleftarrows Ar^{**} + e_s$	$1.05(-8)T_e^{0.71}\exp(-19.7/T_e)\text{cm}^3/\text{s}$	19
$Ar^* + e_s \rightleftarrows Ar^{**} + e_s$	$7.24(-7)T_e^{0.51}\exp(-2.28/T_e)\text{cm}^3/\text{s}$	19
$Ar + e_s \rightarrow Ar^+ + 2e_s$	$1.75(-8)T_e^{0.68}\exp(-23.6/T_e)\text{cm}^3/\text{s}$	19
$Ar^* + e_s \rightarrow Ar^+ + 2e_s$	$5.18(-8)T_e^{0.67}\exp(-6.27/T_e)\text{cm}^3/\text{s}$	19
$Ar^{**} + e_s \rightarrow Ar^+ + 2e_s$	$1.41(-7)T_e^{0.61}\exp(-4.00/T_e)\text{cm}^3/\text{s}$	19
$Ar_2^* + e_s \rightarrow Ar_2^+ + e_s$	$6.78(-8)T_e^{0.70}\exp(-5.25/T_e)\text{cm}^3/\text{s}$	19
$Ar_2^* + e_s \rightarrow 2Ar + e_s$	$1.0(-7)\text{cm}^3/\text{s}$	estimated
$Ar_2^* + e_s \rightarrow Ar_2^{**} + e_s$	$1.0(-7)\text{cm}^3/\text{s}$	17
$Ar_2^{**} + e_s \rightarrow Ar_2^* + e_s$	$1.0(-6)\text{cm}^3/\text{s}$	17
$ArXe^* + e_s \rightarrow ArXe^+ + 2e_s$	$6.60(-8)T_e^{0.71}\exp(-5.40)/T_e)\text{cm}^3/\text{s}$	19
$ArXe^* + e_s \rightarrow Ar + Xe + e_s$	$3.0(-7)\text{cm}^3/\text{s}$	17
$F_2 + e_s \rightarrow F^- + F$	$4.0(-9)T_e^{-1.18}\text{cm}^3/\text{s}$	20
$F_2 + e_s \rightarrow 2F$	$3.0(-10)\text{cm}^3/\text{s}$	21
$F + e_s \rightarrow F^-$	$1.0(-12)\text{cm}^3/\text{s}$	21
Neutral reaction		
$Ar^* + 2Ar \rightarrow Ar_2^* + Ar$	$3.3(-32)\text{cm}^6/\text{s}$	22
$Ar^* + Xe + Ar \rightarrow ArXe^* + Ar$	$1.0(-32)\text{cm}^6/\text{s}$	23
$Xe^* + 2Ar \rightarrow ArXe^* + Ar$	$1.0(-33)\text{cm}^6/\text{s}$	22
$Xe^* + Xe + Ar \rightarrow Xe_2^* + Ar$	$2.3(-32)\text{cm}^6/\text{s}$	25
$Xe^* + 2Xe \rightarrow Xe_2^*(^1\Sigma) + Xe$	$1.7(-32)\text{cm}^6/\text{s}$	24
$Xe^* + 2Xe \rightarrow Xe_2^*(^3\Sigma) + Xe$	$3.0(-32)\text{cm}^6/\text{s}$	24
$ArXe^* + Xe \rightarrow Xe_2^*(^1\Sigma) + Ar$	$3.0(-32)\text{cm}^6/\text{s}$	22
$Ar^{**} + Ar \rightarrow Ar^* + Ar$	$1.0(-10)\text{cm}^3/\text{s}$	19
$Xe^{**} + Ar \rightarrow Xe^* + Ar$	$1.0(-10)\text{cm}^3/\text{s}$	26
$Xe^{**} + Xe \rightarrow Xe^* + Xe$	$1.0(-10)\text{cm}^3/\text{s}$	26
$Ar^* + Xe \rightarrow Xe^* + Ar$	$2.1(-10)\text{cm}^3/\text{s}$	23
$Ar_2^* + Xe \rightarrow Xe^* + 2Ar$	$2.4(-10)\text{cm}^3/\text{s}$	22
$Ar_2^* + Xe \rightarrow ArXe^* + Ar$	$5.0(-11)\text{cm}^3/\text{s}$	estimated
$Xe^* + Xe \rightarrow 2Xe$	$3.5(-15)\text{cm}^3\text{s}$	71
$Xe^{**} + 2Xe \rightarrow Xe_2^{**} + Xe$	$1.0(-31)\text{cm}^6/\text{s}$	17
$Ar^{**} + 2Ar \rightarrow Ar_2^{**} + Ar$	$1.0(-31)\text{cm}^6/\text{s}$	17
$Xe_2^{**} + M \rightarrow Xe^* + Xe + M$	$1.0(-11)\text{cm}^3/\text{s}$	17
$Ar_2^{**} + M \rightarrow Ar^* + Ar + M$	$1.0(-11)\text{cm}^3/\text{s}$	17
$Xe_2^*(^1\Sigma) + M \rightarrow Xe_2^*(^3\Sigma) + M$	$1.3(-13)\text{cm}^3/\text{s}$	27
Penning ionization		
$Xe^* + Xe^* \rightarrow Xe^+ + Xe + e$	$5.0(-10)\text{cm}^3/\text{s}$	29
$Xe_2^* + Xe_2^* \rightarrow Xe_2^+ + 2Xe + e$	$5.0(-10)\text{cm}^3/\text{s}$	29
$Ar^* + Ar^* \rightarrow Ar^+ + Ar + e$	$5.0(-10)\text{cm}^3/\text{s}$	28
$Ar_2^* + Ar_2^* \rightarrow Ar_2^+ + 2Ar + e$	$5.0(-10)\text{cm}^3/\text{s}$	22
Charge transfer		
$Ar^+ + 2Ar \rightarrow Ar_2^+ + Ar$	$2.5(-31)\text{cm}^6/\text{s}$	17
$Ar^+ + Xe + Ar \rightarrow ArXe^+ + Ar$	$1.0(-31)\text{cm}^6/\text{s}$	30
$Xe^+ + 2Ar \rightarrow ArXe^+ + 2Ar$	$1.0(-31)\text{cm}^6/\text{s}$	32

TABLE I. (*continued*).

Reaction	Rate constant	Reference
$Xe^+ + Xe + Ar \rightarrow Xe_2^+ + Ar$	$2.0(-31)cm^6/s$	31
$Xe^+ + 2Xe \rightarrow Xe_2^+ + Xe$	$2.5(-31)cm^6/s$	33
$Ar_2^+ + 2Xe \rightarrow Xe^+ + 2Ar$	$1.0(-9)cm^3/s$	31
$ArXe^+ + Xe \rightarrow Xe_2^+ + Ar$	$1.0(-11)cm^3/s$	34
$ArXe^+ + Xe \rightarrow Xe^+ + Ar + Xe$	$5.0(-10)cm^3/s$	34
Dimer-ion electron recombination		
$Ar_2^+ + e_s \rightarrow Ar^{**} + Ar$	$1.5(-9)(T_g/T_e)^{0.43}cm^3/s$	35
$Xe_2^+ + e_s \rightarrow Xe^{**} + Xe$	$1.5(-8)(T_g/T_e)^{0.5}cm^3/s$	35
$ArXe^+ + e_s \rightarrow Xe^{**} + Ar$	$1.5(-8)(T_g/T_e)^{0.5}cm^3/s$	32
Radiation		
$Xe_2^*(^1\Sigma) \rightarrow 2Xe + h\nu$	$1.82(+8)/s$	36
$Xe_2^*(^3\Sigma) \rightarrow 2Xe + h\nu$	$1.00(+7)/s$	36
$Ar_2^* \rightarrow 2Ar + h\nu$	$6.00(+7)/s$	36
$ArXe^* \rightarrow Ar + Xe + h\nu$	$5.00(+7)/s$	estimated
$Xe^{**} \rightarrow Xe^* + h\nu$	$1.49(+7)/s$	17
$XeF^*(B) \rightarrow XeF(X) + h\nu$	$6.25(+7)/s$	58
$XeF^*(B) + h\nu \rightarrow XeF(X) + 2h\nu$	$4.00(-16)cm^2/s$	50, 58
$XeF^*(C) \rightarrow Xe + F + h\nu$	$9.96(+6)/s$	
$Xe_2F^* \rightarrow 2Xe + F + h\nu$	$6.58(+6)/s$	53, 54
$ArF^* \rightarrow Ar + F + h\nu$	$2.38(+8)/s$	56
$Ar_2F^* \rightarrow 2Ar + F + h\nu$	$4.40(+6)/s$	47
Ion-ion recombination		
$Xe^+ + F^-(+M) \rightarrow XeF^*(B)(+M)$	Pressure-dependent	
$Xe_2^+ + F^-(+M) \rightarrow XeF^*(B) + Xe(+M)$		
$Ar^+ + F^-(+M) \rightarrow ArF^*(+M)$	rate constant	9
$Ar_2^+ + F^-(+M) \rightarrow XeF^* + Ar(+M)$		
$ArXe^+ + F^-(+M) \rightarrow XeF^*(B) + Ar(+M)$		
Neutral formation		
$Xe^* + F_2 \rightarrow XeF^*(B) + F$	$7.5(-10)cm^3/s$	37
$Xe^{**} + F_2 \rightarrow XeF^*(B) + F$	$7.5(-10)cm^3/s$	38
$Xe_2^* + F_2 \rightarrow XeF^*(B) + Xe + F$	$5.0(-10)cm^3/s$	39
$Xe_2^* + F_2 \rightarrow Xe_2F^* + F$	$2.5(-10)cm^3/s$	40
$Xe_2^{**} + F_2 \rightarrow Xe_2F^*(B) + Xe + F$	$5.0(-10)cm^3/s$	41
$Xe_2^{**} + F_2 \rightarrow Xe_2F^* + F$	$2.5(-10)cm^3/s$	42
$Ar^* + F_2 \rightarrow ArF^* + F$	$1.6(-9)cm^3/s$	37
$Ar^{**} + F_2 \rightarrow ArF^* + F$	$1.6(-9)cm^3/s$	45
$Ar_2^* + F_2 \rightarrow ArF^* + Ar + F$	$5.2(-10)cm^3/s$	46
$Ar_2^* + F_2 \rightarrow Ar_2F^* + F$	$2.5(-10)cm^3/s$	47
$Ar_2^{**} + F_2 \rightarrow ArF^* + Ar + F$	$5.2(-10)cm^3/s$	45
$Ar_2^{**} + F_2 \rightarrow Ar_2F^* + F$	$2.5(-10)cm^3/s$	45
$ArXe^* + F_2 \rightarrow XeF^*(B) + Ar + F$	$5.0(-10)cm^3/s$	39
Displacement XeF* formation		
$ArF^* + Xe \rightarrow XeF^*(B) + Ar$	$1.6(-9)cm^3/s$	43
$Ar_2F^* + Xe \rightarrow XeF^*(B) + 2Ar$	$2.0(-10)cm^3/s$	44
Xe_2F^* relaxation		
$Xe_2F^* + Xe \rightarrow 3Xe + F$	$1.0(-13)cm^3/s$	53, 54
$Xe_2F^* + Ar \rightarrow 2Xe + F + Ar$	$2.8(-14)cm^3/s$	53, 54
$Xe_2F^* + F_2 \rightarrow 2Xe + 3F$	$2.0(-10)cm^3/s$	70
$Xe_2F^* + e_s \rightarrow 2Xe + F + e_s$	$1.0(-7)cm^3/s$	estimated
Ar_2F^* relaxation		
$Ar_2F^* + Ar \rightarrow 3Ar + F$	$2.8(-13)cm^3/s$	47
$Ar_2F^* + F_2 \rightarrow 2Ar + 3F$	$2.0(-10)cm^3/s$	57
$Ar_2F^* + e_s \rightarrow Ar + F + e_s$	$1.0(-7)cm^3/s$	estimated
ArF^* relaxation		
$ArF^* + Ar \rightarrow 2Ar + F$	$8.6(-12)cm^3/s$	43
$ArF^* + F_2 \rightarrow Ar + 3F$	$1.8(-9)cm^3/s$	57
$ArF^* + e_s \rightarrow Ar + F + e_s$	$1.6(-7)cm^3/s$	55
$ArF^* + 2Ar \rightarrow 3Ar + F$	$5.0(-31)cm^3/s$	47
$XeF^*(B)$ relaxation	[$XeF^*(C)$ relaxation: see text]	
$XeF^*(B) + Xe \rightarrow 2Xe + F$	$3.3(-11)cm^3/s$	58
$XeF^*(B) + Ar \rightarrow Xe + F + Ar$	$4.9(-12)cm^3/s$	49
$XeF^*(B) + F_2 \rightarrow Xe + 3F$	$3.8(-10)cm^3/s$	58
$XeF^*(B) + e_s \rightarrow Xe + F + e_s$	$1.5(-7)cm^3/s$	estimated
$XeF^*(B) + 2Xe \rightarrow Xe_2F + Xe$	$2.6(-31)cm^6/s$	48

TABLE I. (*continued*).

Reaction	Rate constant	Reference
$XeF^*(B) + Xe + Ar \rightarrow Xe_2F + Ar$	$3.0(-31)cm^6/s$	50
$XeF^*(B) + 2Ar \rightarrow Xe + F + 2Ar$	$7.2(-32)cm^6/s$	49
Absorption		
$Xe^* + h\nu \rightarrow Xe^+$	$2.2(-19)cm^2$	59
$Xe^{**} + h\nu \rightarrow Xe^+$	$1.0(-17)cm^2$	60
$Xe_2^* + h\nu \rightarrow Xe_2^+$	$1.0(-19)cm^2$	61
$Xe_2^{**} + h\nu \rightarrow Xe_2^+$	$1.0(-17)cm^2$	estimated
$Xe_2^+ + h\nu \rightarrow Xe^+ + Xe$	$3.3(-17)cm^2$	62
$Ar^* + h\nu \rightarrow Ar^+$	$1.1(-19)cm^2$	59
$Ar^{**} + h\nu \rightarrow Ar^+$	$1.0(-17)cm^2$	60
$Ar_2^* + h\nu \rightarrow Ar_2^+$	$1.9(-19)cm^2$	63
$Ar_2^{**} + h\nu \rightarrow Ar_2^+$	$1.0(-17)cm^2$	estimated
$Xe_2^* + h\nu \rightarrow Ar^+ + Ar$	$1.3(-17)cm^2$	62
$ArXe^* + h\nu \rightarrow ArXe^+$	$1.0(-19)cm^2$	61
$ArXe^* + h\nu \rightarrow Xe^+ + Ar$	$1.0(-17)cm^2$	64
$F_2 + h\nu \rightarrow 2F$	$5.3(-21)cm^2$	65
$F^- + h\nu \rightarrow F + e$	$2.2(-18)cm^2$	66
$XeF^*B \rightleftarrows C$ interconversion		
$XeF^*(B) + Xe \rightleftarrows XeF^*(C) + Xe$	$4.7(-10)cm^3/s$	estimated
$XeF^*(B) + Ar \rightleftarrows XeF^*(C) + Ar$	$2.4(-12)cm^3/s$	estimated
$XeF^*(B) + F_2 \rightleftarrows XeF^*(C) + F_2$	$2.4(-11)cm^3/s$	estimated
$XeF^*(B) + e \rightleftarrows XeF^*(C) + e$	$1.0(-7)cm^3/s$	estimated
XeF(X)lifetime		
$XeF(X) \rightarrow Xe + F$	$2.0(-9)$s at 300 K, 1atm	estimated

the presence of the closely lower-lying C state must be taken into account because of collisional mixing of the B and C states. Numbers of 4.7×10^{-10}, 2.4×10^{-12}, 2.4×10^{-11}, and 1.0×10^{-7} cm^3/s are used in the calculation for the reactions of $XeF^*(B) + M \rightleftarrows XeF^*(C) + M$: M = Xe, Ar, F_2, and secondary electrons, respectively. Since the vibrational relaxation rates in the B and C states are relativey slow, these should also be taken into account. In the calculation a number of 3×10^{-11} cm^3/s reported by Lorents[71] is used as the vibrational relaxation rates. An accurate model for the B, C, and X states is necessary because these states directly affect laser performance.

There are a few laser transitions between $v' = 0$ and 1 levels of the B state and $v'' = 2$, 3, 4, and 6 levels of the X state[6,72]; e.g., $v' = 0$ (B state) $\rightarrow v'' = 3$ (X state) is a major laser transition at room temperature. However, in order to simplify the model, we treated these transitions as a single laser transition because this model was mainly developed to describe the laser output power and enegy, and not to investigate the spectral characteristics.

Figure 3 shows in detail the upper B and C states assumed in our model. Four vibrational levels, i.e., $v = 0$ and 1, 2, 3, and a reservoir, and seven vibrational levels, i.e., $v = 0$, 1, 2, 3, 4, 5, and a reservoir were considered in the B and C states, respectively. The $v = 0$ and 1 levels of the B state are treated as a single level, and high vibrational levels are treated together as the reservoir. Furthermore, it is assumed that all the initially formed XeF* molecules are in the B state, and 40%, 20%, 20%, and 20% of the excited molecules are in the reservoir, $v = 3$, 2, and 0 and 1 levels, respectively.[71] Since the energy difference ($E_C - E_B = -775$ cm^{-1})[73] between the B and the C states at the bottom of the potential curve is exceptionally large in comparison to the other rare-

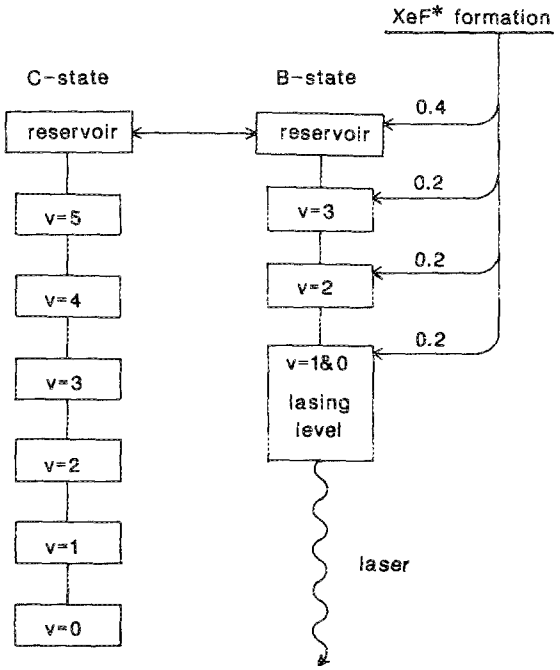

FIG. 3. Upper state model of XeF laser with considerations of vibrational relaxation and the B-C mixing process.

gas halide excimers, the B-C mixing is assumed to occur only between the reservoirs.

The bonding energy in the X state is also much larger ($D_e = 1175\ \text{cm}^{-1}$)[74] than that of the other rare-gas halide excimers, and the lower levels of the XeF($B \rightarrow X$) laser transitions are near the bottom of the energy potential curve ($v'' = 2$, 3, 4, and 6). Therefore, the XeF($B \rightarrow X$) laser performance depends on the number densities of molecules in the $v'' = 2$, 3, 4, and 6 levels which vary with vibrational relaxations and collisional dissociations. The rates for these reactions were reported in detail by Fulghum, Feld, and Javan,[75] Wilkins,[76] and Bott *et al.*[77] The vibrational relaxation and dissociation rates in the X state can be combined, and the decay rate of the X state was described in terms of the lifetime. Since the vibrational relaxation rates or the dissociation rates depend on gas temperatures, the lifetime was treated as a function of gas temperature.

The XeF* electron quenching rate affects the laser output dependence of F_2 or Xe fractions in the laser gas mixtures (see Fig. 5). Quenching rate coefficients for XeF*(B) of 7×10^{-8} cm^3/s (Ref. 78) (obtained theoretically) and 4×10^{-7} cm^3/s (Ref. 48) (obtained experimentally) were reported. However, we use 1.5×10^{-7} cm^3/s for the rate coefficient because this value has been successfully applied to simulation codes for other rare-gas halide excimer lasers.

III. VALIDATION OF THE COMPUTER MODEL

The validity of the simulation code was confirmed by comparing the computed results to those obtained in a previously reported experiment.[8] The sidelight waveforms obtained from calculations and in the experiment are shown in Fig. 4 together with the e-beam-current pulse waveform. The conditions used in the calculation are the same as those of the experiment. Because these results show agreement in rise time and pulse width, the model for XeF*(B) formation and quenching channels must be valid.

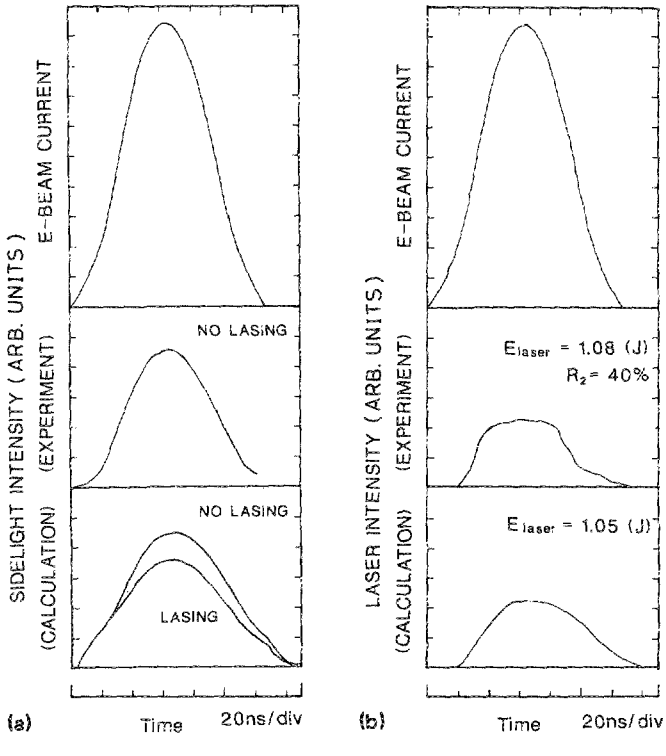

FIG. 4. Comparison of the calculated (a) XeF($B \rightarrow X$) fluorescence and (b) laser waveform with experimental result. The mixture was composed of Ar/Xe/F_2 = 93.2/6.0/0.8% at a total pressure of 711 Torr and excitation rate of 1.1 MW/cm^3.

Figure 4 also shows a comparison of the laser waveform obtained from theory and the previous experiment. Both results agree and confirm the model for the X state.

Figure 5 shows a comparison of dependence of the laser energy on fractions of Xe and F_2, and the total pressure between calculated results and experiment. The conditions are shown in each figure. The calculated results agree well with the experimental results in each case. From these results it is possible to conclude that our model is valid to investigate the temporal evolution of both laser intensity and energy.

IV. RESULTS AND DISCUSSION

A theoretical analysis was conducted using a simulation code to optimize the short-pulse e-beam-pumped XeF($B \rightarrow X$) laser performance for total pressure and pumping density. In the calculation of Fig. 4, it was found that the saturation intensity I_s is small ($I_s \sim 0.5$ MW/cm^2). Therefore, the gain saturates early in the pumping period. In Ar/Xe/F_2 laser gas mixtures, the photoabsorption cross sections of the products from the diluent gas, i.e., rare-gas dimer ions, rare-gas dimers, and excited rare gases, are 10–100 times larger than those in conventional Ne/Xe/NF_3 mixtures. Especially, the rare-gas dimer ions and the rare-gas dimers are the major photoabsorbers in the XeF laser kinetics. Since these absorbers are formed through three-body collisional reactions, the absorption increases proportionally to the square of the total pressure. On the other hand, the ion-ion recombination, which is the major reaction to form XeF*, is also a three-body reaction, which is not proportional to the square of the total pressure.[79] The maximum reaction rate for the Ar diluent is obtained at 1–2 atm. Therefore, the extraction and intrinsic efficiency can be improved at a low total gas pressure (< 1 atm) when the absorbers decrease while the XeF* formation does not.

A 60-cm-length intracavity model (50-cm-long excitation region along the optical path) is used for this analysis in order to reduce the absorption by F_2 and the resonator losses from optical windows (in the calculation of Figs. 4 and 5, the losses from windows are taken into account). The e-beam waveform used in the calculation is the same as that used in the experiments (see Fig. 4). The subsequent calculations are conducted with optimized values of the Xe and F_2 fraction and the output coupling, e.g., 18% Xe, 1.4% F_2, and 70% coupling for 1.2-MW/cm^3 excitation rate at total pressure of 0.5 atm.

The calculated specific laser energy and the intrinsic efficiency with the same excitation rate as that of the experiment (1.14 MW/cm^3, 65 ns FWHM at 711 Torr) are shown in Fig. 6. The maximum intrinsic efficiency of $\sim 3\%$ is obtained at a low total pressure (0.5 atm). Figure 7 shows the calculated small signal gain g_0, absorption α, and g_0/α for the same conditions as in Fig. 6. With increasing total pres-

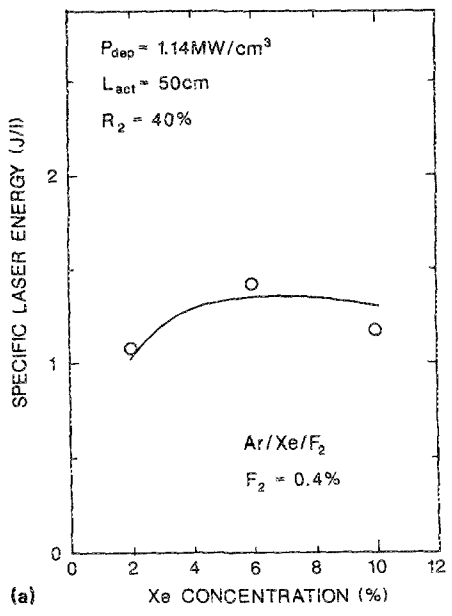

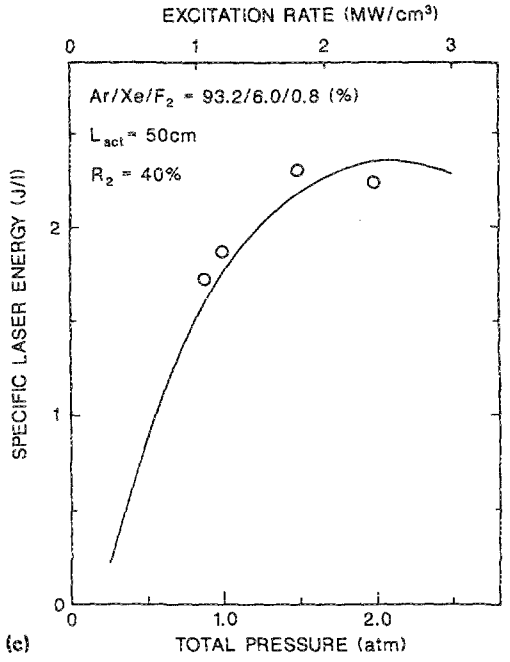

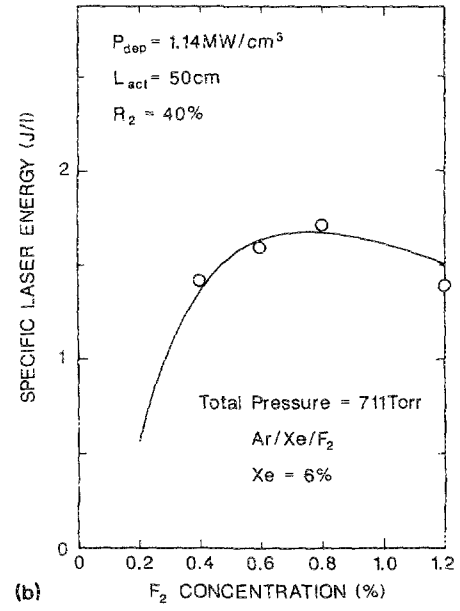

FIG. 5. Comparison of the laser output energy obtained from theory (solid lines) and experiment (open circles) as a function of (a) Xe concentration, (b) F_2 concentration, and (c) total gas pressure. The excitation rate is 1.1 MW/cm³ and the output coupler reflectivity, $R_2 = 40\%$.

sure, g_0 saturates and α increases, and consequently g_0/α decreases. The ratio g_0/α also decreases below 0.5-atm total pressure, because the absorption by F_2 increases for this total pressure range. The formation rate of XeF* and the extraction efficiency are shown in Fig. 8 as a function of the total pressure. The formation rate below 0.5 atm is even higher than that at 0.5 atm with optimization of the laser gas mixture. As a result, the intrinsic efficiency depends somewhat on the total gas pressure, and the maximum value is obtained in the range of 0.5–0.7 atm.

Figure 9 shows the intrinsic efficiencies as a function of the excitation rate for various total pressures. It should be noted that the unit of the excitation rate is in MW/cm³ atm. Therefore, the dependence of laser energy on total gas pressure in a laser can be seen easily. Constant efficiencies can be obtained for a broad excitation rate (0.5–2 MW/cm³ atm).

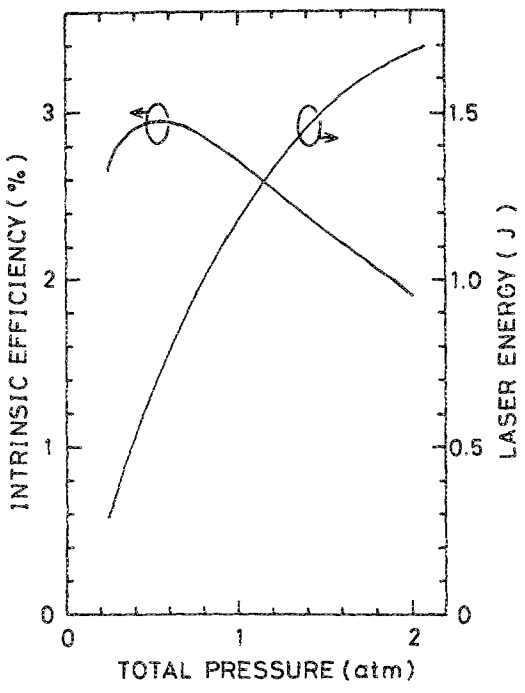

FIG. 6. Calculated specific laser output energy and intrinsic efficiency η_{int} as a function of total gas pressure.

The maximum intrinsic efficiency of 3% is as high as that obtained with $Ne/Xe/NF_3$ gas mixtures at room temperature.

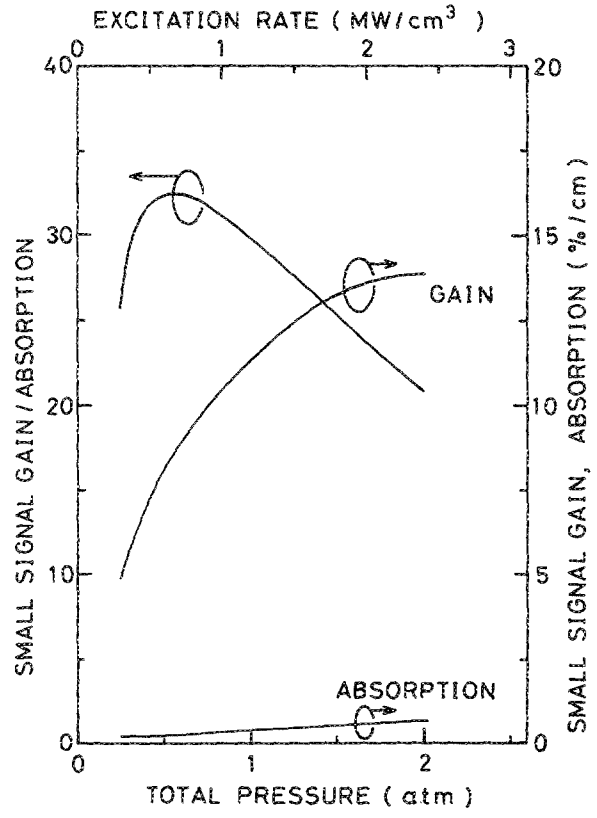

FIG. 7. Calculated small signal gain g_0, absorption coefficient α, and g_0/α as a function of total gas pressure.

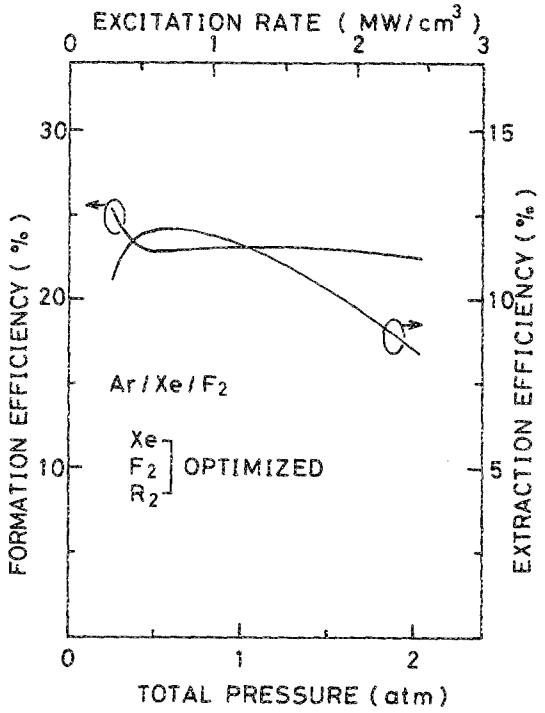

FIG. 8. Calculated formation efficiency η_{form} and extraction efficiency η_{ext} as a function of total gas pressure.

V. CONCLUSION

We have developed the computer-simulation code for a short-pulse *e*-beam-excited $XeF(B \rightarrow X)$ laser operating with $Ar/Xe/F_2$ laser gas mixtures. This simulation code shows good agreement with the results of a previous experiment.[8]

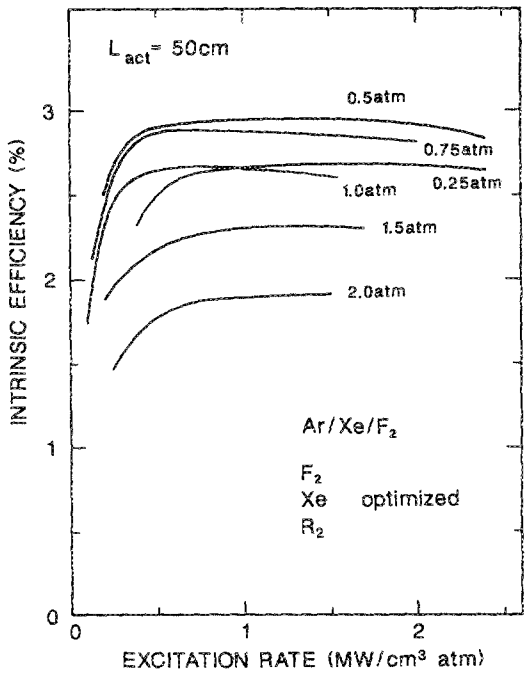

FIG. 9. Calculated intrinsic efficiency η_{int} as a function of excitation rate (MW/cm³ atm) at various total gas pressures of 0.25, 0.5, 0.75, 1.0, 1.5, and 2.0 atm.

The calculation suggests that a maximum intrinsic efficiency of almost 3% can be obtained at room temperature with the $Ar/Xe/F_2$ mixture which previously has been considered not suitable for the $XeF(B \rightarrow X)$ laser because of its photoabsorptions and high quenching rates for XeF*. The result was obtained with a low total gas pressure (< 1 atm) where the formation of major absorbers (rare-gas dimers and dimer ions) is small and the extraction efficiency is high. Also, it is found that this highly efficient operation can be obtained for a wide total pressure range (0.4–0.8 atm) and excitation rate range (0.5–2.0 MW/cm^3 atm).

Consequently, this study shows that short-pulse *e*-beam-excited $XeF(B \rightarrow X)$ lasers can be effectively scaled with a low-total-pressure $Ar/Xe/F_2$ gas mixture at room temperature, which is more convenient than a conventional high-total-pressure $Ne/Xe/NF_3$ gas mixture at elevated temperatures.

[1]E. R. Ault, R. S. Bradford, Jr., and M. L. Bhaumik, Appl. Phys. Lett. **27**, 413 (1975).
[2]L. F. Champagne and N. W. Harris, Appl. Phys. Lett. **31**, 513 (1977).
[3]J. C. Hsia, J. A. Mangano, J. H. Jacob, and M. Rokni, Appl. Phys. Lett. **34**, 208 (1979).
[4]W. D. Kimura, S. E. Moody, and J. F. Seamans, Appl. Phys. Lett. **49**, 255 (1986).
[5]L. Litzenberger and A. Mandl, Appl. Phys. Lett. **52**, 1557 (1988).
[6]A. Mandl and L. Litzenberger, Appl. Phys. Lett. **51**, 955 (1987).
[7]M. Obara, T. Fujioka, F. Kannari, and A. Suda, Proc. SPIE **476**, 6 (1984).
[8]N. Nishida, F. K. Tittel, H. Kumagai, Y. W. Lee, and M. Obara, Appl. Phys. Lett. **52**, 1847 (1988).
[9]J. M. Hoffmann and J. B. Moreno, Sandia National Laboratories Report, SAND80-1486, 1980 (unpublished).
[10]A. E. Mandl and H. A. Hyman, IEEE J. Quantum Electron. **QE-22**, 349 (1986).
[11]W. D. Kimura and J. F. Seamans, IEEE J. Quantum Electron. **QE-24**, 2121 (1988).
[12]T. H. Johnson, L. J. Palumbo, and A. M. Hunter II, IEEE J. Quantum Electron. **QE-15**, 289 (1979).
[13]J. A. Blauer, T. P. Yang, C. E. Turner, and D. A. Copeland, Appl. Opt. **23**, 4352 (1984).
[14]T. J. Moratz, T. D. Sawnders, and M. J. Kushner, J. Appl. Phys. **64**, 3799 (1988).
[15]F. Kannari, A. Suda, M. Obara, and T. Fujioka, IEEE J. Quantum Electron. **QE-19**, 1587 (1983).
[16]J. G. Christphorou, *Atomic and Molecular Radiation Physics* (Wiley, New York, 1971).
[17]D. C. Lorents, Physica **82C**, 19 (1976).
[18]L. A. Levin, S. A. Moody, E. L. Klosterman, R. E. Center, and J. J. Ewing, IEEE J. Quantum Electron. **QE-17**, 2282 (1981).
[19]"Conceptional design of a KrF scaling module," final report by MSNW Incorporated, Contract De-ACO(079DP0115, 1980) (unpublished).
[20]D. W. Trainor and J. H. Jacob, Appl. Phys. Lett. **35**, 920 (1979).
[21]T. H. Johnson and A. M. Hunter II, J. Appl. Phys. **51**, 2406 (1980).
[22]C. A. Brau, in *Excimer Lasers*, edited by C. K. Rhodes (Springer, Berlin, 1979).
[23]Analogous to $Ar^* + Kr + Ar \rightarrow ArKr^* + Ar$; H. H. Nakano, R. M. Hill, D. C. Lorents, D. L. Huestis, and M. V. McCusker, SRI International Reserach Report MP76-99, 1976 (unpublished).
[24]B. E. Cherrington, *Gaseous Electronics and Gas Lasers* (Pergamon, Oxford, 1979).
[25]J. K. Rice and A. W. Johnson, J. Chem. Phys. **63**, 5235 (1975).
[26]Analogous to $Ar^{**} + Ar \rightarrow Ar^* + Ar$; see Ref. 19.
[27]C. Duzy and J. Boness, IEEE J. Quantum Electron. **QE-16**, 638 (1980).
[28]P. K. Leichner and R. J. Ericson, Phys. Rev. A **9**, 251 (1974).
[29]J. B. Laudenslager, in *Kinetics of Ion-molecule Reactions*, edited by P. Ausloos (Plenum, New York, 1979).
[30]Analogous to $Ne^+ + Xe + Ne \rightarrow NeXe^+ + Ne$; see Ref. 18.
[31]S. J. J. Nagalingam and G. H. Miley, presented at Topical Meeting on Eximer Lasers, Charleston, South Carolina, 1979.
[32]J. Boker and C. K. Rhodes, J. Chem. Phys. **73**, 2626 (1980).
[33]D. C. Lorents, D. J. Eckstrom, and D. L. Heustis, SRI International Research Report MP73-2 (AD-778-326), 1973 (unpublished).
[34]Analogous to $NeKr^+ + Kr$; H. L. Kramer, J. A. Herce, and E. E. Muschlitz, Jr., J. Chem. Phys. **56**, 4166 (1972).
[35]H. J. Oskam and V. R. Mittelstadt, Phys. Rev. **132**, 1455 (1963).
[36]J. W. Keto, R. E. Gleason, Jr., and G. K. Walters, Phys. Rev. Lett. **33**, 1365 (1974).
[37]J. E. Velazco, J. H. Koltz, and D. W. Setser, J. Chem. Phys. **65**, 3468 (1976).
[38]Analogous to $Xe^* + F_2 \rightarrow XeF^* + F$.
[39]Estimated from Ar_2^*; C. H. Chen, M. G. Payne, and J. P. Judish, J. Chem. Phys. **69**, 1626 (1978).
[40]Estimated from Ar_2^*; some of Ar_2^* quenched by F_2 seems to produce Ar_2F^*; G. Marowsky, G. P. Glass, F. K. Tittel, K. Hohla, W. L. Wilson, Jr., and H. Weber, IEEE J. Quantum Electron. **QE-18**, 898 (1982). The rate constant is assumed to be analogous to $Ar_2^* + NF_3 \rightarrow Ar_2F^* + NF_2$; N. Boewering, R. Sauerbrey, and H. Langhof, J. Chem. Phys. **76**, 3524 (1982).
[41]Analogous to $Xe_2^* + F_2 \rightarrow XeF^* + Xe + F$.
[42]Analogous to $Xe_2^* + F_2 \rightarrow XeF^* + F$.
[43]M. Rokni, J. H. Jacob, J. A. Mangano, and R. Brochu, Appl. Phys. Lett. **31**, 79 (1977).
[44]Y. Nachshon, F. K. Tittel, and W. L. Wilson, Jr., J. Appl. Phys. **56**, 36 (1984).
[45]Analogous to Ar.
[46]C. H. Chen, M. G. Payne, and J. P. Judish, J. Chem. Phys. **69**, 1626 (1978).
[47]N. Boewering, R. Sauerbrey, and H. Langhof, J. Chem. Phys. **76**, 3524 (1982).
[48]D. W. Trainor, J. H. Jacob, and M. Rokni, J. Chem. Phys. **72**, 3646 (1980).
[49]J. G. Eden and R. W. Waynant, Opt. Lett. **2**, 13 (1978).
[50]M. Rokni, J. H. Jacob, J. A. Mangano, and R. Brochu, Appl. Phys. Lett. **30**, 458 (1977).
[51]Based on Refs. 2 and 50.
[52]J. E. Velazco and D. W. Setser, J. Chem. Phys. **62**, 1990 (1975).
[53]W. Walter, R. Sauerbrey, F. K. Tittel, and W. L. Wilson, Jr., Appl. Phys. Lett. **41**, 387 (1982).
[54]R. Sauerbrey, W. Walter, F. K. Tittel, and W. L. Wilson, Jr., J. Chem. Phys. **78**, 735 (1983).
[55]D. W. Trainor and J. H. Jacob, Appl. Phys. Lett. **37**, 675 (1980).
[56]T. H. Dunning, Jr., and P. J. Hay, J. Chem. Phys. **69**, 134 (1978).
[57]G. Marowsky, G. P. Glass, F. K. Tittel, K. Hohla, W. L. Wilson, Jr., and H. Weber, IEEE J. Quantum Electron. **QE-18**, 898(1982).
[58]J. G. Eden and R. W. Waynant, J. Chem. Phys. **68**, 2850 (1978).
[59]K. J. McCann and M. R. Flannery, Appl. Phys. Lett. **31**, 599 (1977).
[60]C. Duzy and H. A. Hyman, Phys. Rev. A **22**, 1878 (1980).
[61]Estimated from Ar_2^*.
[62]W. R. Wadt, J. Chem. Phys. **73**, 3915 (1980).
[63]R. Sauerbrey, IEEE J. Quantum Electron. **QE-23**, 5 (1987).
[64]Estimated from AR_2^+ and Xe_2^+.
[65]R. K. Steunenberg and R. C. Vogel, J. Am. Chem. Soc. **78**, 901 (1956).
[66]A. Mandl, Phys. Rev. A **3**, 251 (1971).
[67]W. Wiemic, J. Phys. B **7**, 850 (1974).
[68]Analogous to $Ar_2F^* + F_2$; G. Marowsky, G. P. Glass, F. K. Tittel, K. Hohla, W. L. Wilson, Jr., and H. Weber, IEEE J. Quantum Electron. **QE-18**, 898 (1982).
[69]C. J. Elliott and A. E. Greene, J. Appl. Phys. **47**, 2946 (1976).
[70]C. W. Werner, E. V. George, and P. W. Hoff, IEEE J. Quantum Electron. **QE-13** 769 (1977).
[71]D. C. Lorents, SRI International Research Report No. MP83-142, 1983 (unpublished).
[72]J. Tellinghuisen and P. C. Tellinghuisen, J. Chem. Phys. **68**, 5177 (1978).
[73]H. Helm, D. L. Huestis, M. J. Dyer, and D. C. Lorents, J. Chem. Phys. **79**, 3220 (1983).
[74]P. C. Tellinghuisen and J. Tellinghuisen, J. Chem. Phys. **68**, 5187 (1978).
[75]S. F. Fulghum, M. S. Feld, and A. Javan, IEEE J. Quantum Electron. **QE-16**, 815 (1980).
[76]R. L. Wilkins, J. Chem. Phys. **89**, 6267 (1988).
[77]J. F. Bott, R. F. Heidner, J. S. Holloway, J. B. Koffend, and M. A. Kwok, J. Chem. Phys. **89**, 4154 (1988).
[78]A. U. Hazi, T. N. Rescigno, and A. E. Orel, Appl. Phys. Lett. **35**, 477 (1979).
[79]M. R. Flannery and T. P. Yang, Appl. Phys. Lett. **32**, 327 (1978).